Solvatochromism based on structural color

Dong, Xu; Wu, Pan; Schaefer, Christian G.; Zhang, Liwu; Finlayson, Christopher; Wang, Changchun

Published in:
Materials and Design

DOI:
10.1016/j.matdes.2018.09.026

Publication date:
2018

Citation for published version (APA):
Dong, X., Wu, P., Schaefer, C. G., Zhang, L., Finlayson, C., & Wang, C. (2018). Solvatochromism based on structural color: Smart polymer composites for sensing and security. *Materials and Design*, *160*, 417-426. https://doi.org/10.1016/j.matdes.2018.09.026

Accepted Manuscript

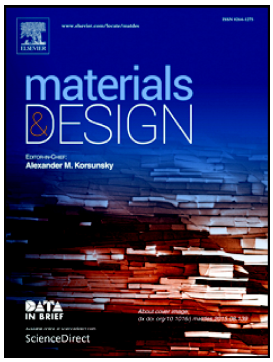

Solvatochromism based on structural color: Smart polymer composites for sensing and security

Xu Dong, Pan Wu, Christian G. Schaefer, Liwu Zhang, Chris E. Finlayson, Changchun Wang

PII: S0264-1275(18)30720-2
DOI: doi:10.1016/j.matdes.2018.09.026
Reference: JMADE 7387

To appear in: *Materials & Design*

Received date: 23 August 2018
Revised date: 10 September 2018
Accepted date: 11 September 2018

Please cite this article as: Xu Dong, Pan Wu, Christian G. Schaefer, Liwu Zhang, Chris E. Finlayson, Changchun Wang , Solvatochromism based on structural color: Smart polymer composites for sensing and security. Jmade (2018), doi:10.1016/j.matdes.2018.09.026

Article type: Original Article

Solvatochromism based on Structural Color: Smart Polymer Composites for Sensing and Security

Xu Dong, Pan Wu, Christian G. Schaefer, Liwu Zhang, Chris E. Finlayson, and Changchun Wang**

Dr. Xu Dong, Pan Wu, Dr. Christian G. Schaefer, and Prof. Changchun Wang
State Key Laboratory of Molecular Engineering of Polymers, Department of Macromolecular Science, and Laboratory of Advanced Materials, Fudan University, 220 Handan Road, Shanghai, 200433, China
*E-mail: ccwang@fudan.edu.cn

Dr. Chris E. Finlayson
Department of Physics, Prifysgol Aberystwyth University, Aberystwyth SY23 3BZ, Wales, U.K.
*E-mail: cef2@aber.ac.uk

Prof. Liwu Zhang
Department of Environnental Science and Engineering, Fudan University, 2205 Songhu Road Shanghai, 200438, China

Keywords: polymer composites, core-shell particles, photonic crystals, stimuli-responsiveness, structural colors

Highlights:

- Large-area transparent photonic crystal (TPC) films of polymer core-shell particles have been engineered with iso-refractive balance of indices.
- TPCs be completely and reversibly switched, between transparency and an intense structurally colored state (10% reflectance), by solvent environment stimuli.
- Cross-linking generates encrypted patterns, revealed via a solvatochromic mechanism, with applications including in sensing and anti-counterfeit security.

Abstract: We report a convenient and scalable strategy to achieve large-area transparent photonic crystal (TPC) films that can be fully reversibly switched between an initial transparent state and a structurally-colored state. This photonic material is based on an ordered colloidal crystal structure of polymer core-shell particles with an engineered refractive index balance of the core and the shell components. Highly transparent viscoelastic quasi-solid films are created that can be spatially UV-cross-linked, giving invisible encrypted photonic patterns with different solvent response compared to non-cross-linked regions, which appear after immersion in solvent media, thus demonstrating clear and fully

reversible/switchable solvatochromic properties. Our intuitive simulation models demonstrate how the emergence of structural colour occurs due to increasing refractive-index contrast, whereas wavelength shifting originates from commensurate solvent swelling of the shell medium. In addition to the very clear revelation of optical patterns (large fractional changes in reflectance, from transparency to a resonant reflectivity of ~10%), these materials and thin-film generation methods are inherently scalable, robust and versatile. The demonstrated stimuli-responsive photonic films may thus give rise to new practicable applications in the fields of environmental sensing and product security.

Graphical Abstract

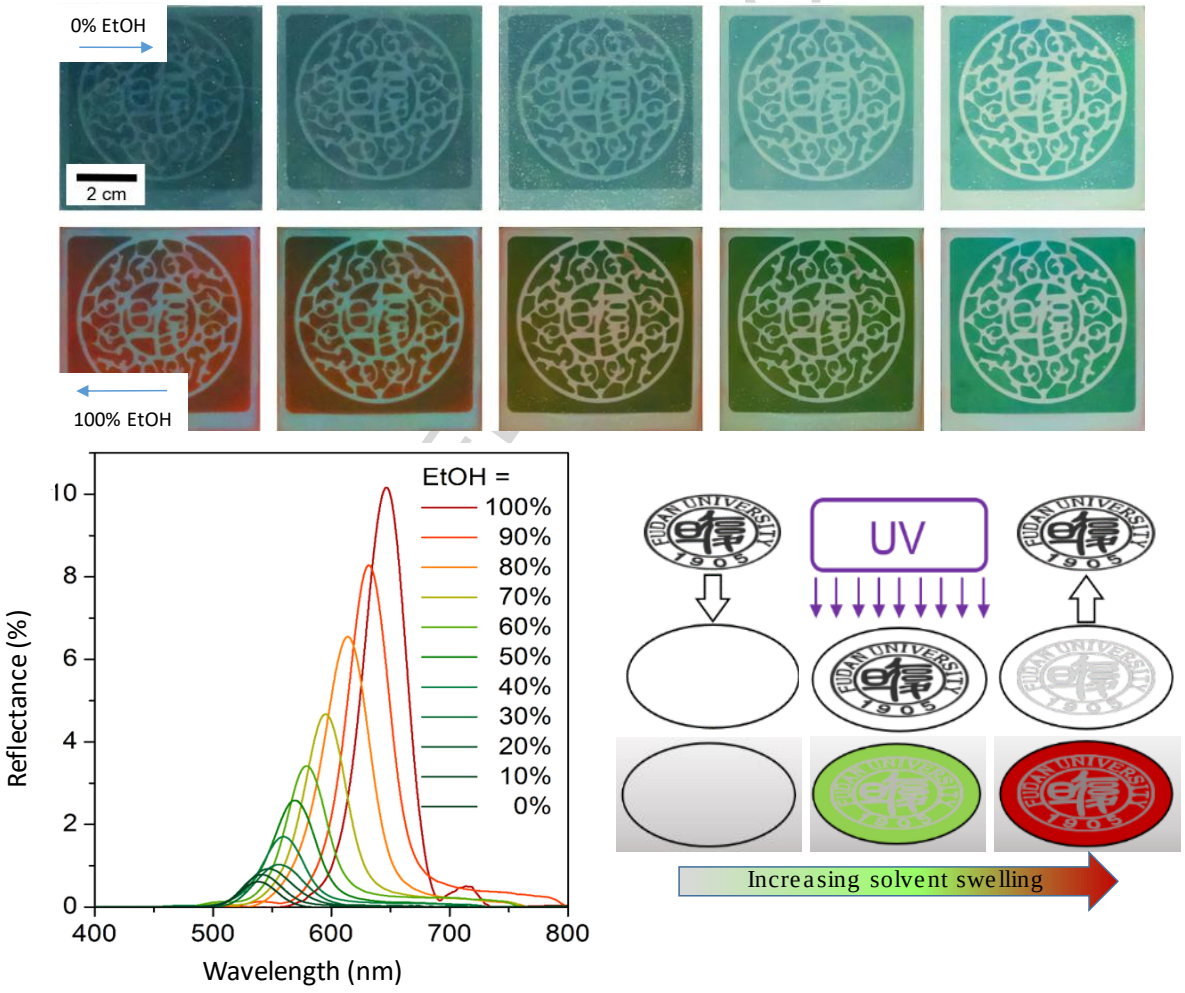

1. Introduction

A common method to prevent counterfeiting of bank notes, passports, credit cards, brand labels and other security documents is to provide them with special color features to enable convenient optical identification.[1-3] The most widely used optical materials for security

applications are dynamic materials, whose color changes with orientation relative to the observer. Whilst many materials exhibit a color change with a variation of the viewing angle, materials which change color reversibly under stimulus, thus enabling and disabling hidden security features, are rather scarce. Relevant environmental stimuli might include change of the ambient temperature, selective chemical wetting, electric or magnetic field manipulation, or mechanical stress.

A very important class of dynamic colored materials, so-called colloidal photonic crystals, which show angle-dependent colors in the visible, can be obtained by the self-assembly of monodispersed, sub micrometer-sized particles.[4-7] Such particles usually crystallize in a face-centered cubic (fcc) lattice structure, and the interstices of the crystal might be filled by a liquid, air, or a second solid phase. An important prerequisite is that a difference in the refractive index between the particles and the matrix material filling the interstices remains, which leads to resonant scattering of light from the underlying 3D structure, accompanied with vivid angle-dependent colorful light reflections, also referred to as structural colors. Thus, the resulting optical properties are determined by the lattice constant of the crystal and by the refractive index contrast between the particles and the surrounding material.[8] High index-contrast (Δn) crystals, mostly derived from solution-based sedimental colloids, can indeed produce impressive resonant reflectivities.[9, 10] However, in keeping with the paradigms of the present study, more realistic attempts at scalable, manufacturable and tractable/transferable structural-color systems necessarily involve “soft-matter” approaches (e.g. using polymers or polymer-composites), where the index-contrast may be at least an order of magnitude lower.

Photonics materials generally have been seen over the last decade as a pioneering area in terms of applications in sensing, bio-sensing and display devices.[11] Many of the underlying strategies have been highly interdisciplinary and wide-ranging; from engineered materials based around the evolutionary self-assembled structures in nature,[12, 13] to integrated sensor engineering.[14, 15] Of particular relevance to the present study, so-called stimuli-responsive colloidal photonic crystals have attracted a great deal of attention due to their reversibly switchable structural colors upon application of various external triggers, such as ions, pH, solvents, redox reagents, electric or magnetic fields. These produce reversible changes of the lattice structure and/or the refractive index contrast, thus inducing reversible changes of the structural color.[16-18] These stimuli-responsive optical materials are interesting candidates for sensing devices,[19, 20] color displays,[21, 22] photonic printing systems,[23-25]

photonic inks and paper.[26-28] Notably, whilst the preparation of stimuli-responsive colloidal photonic crystals are widely described in the scientific literature, examples include using innovative nanolithography,[29] inkjet printing,[30-32] and hydrogel deposition methods,[33] significant industrial production or applications have so far not been effectively realized. More recently, structured materials based on self-organisation at the molecular level, such as with cholesteric liquid crystals,[34, 35] have also become another interesting competing technology to more "monolithic" top-down routes[36] to photonic materials.

However, this type of photonic materials is of special interest for anti-counterfeiting or the storage of secret information.[37, 38] Such materials are particularly suited for use as dynamic security features, in which hidden information in the form of encrypted images or characters can be selectively revealed once an external stimulus is applied. So far, many different anti-counterfeit devices have been realized that are based on the selective visualization of encrypted images under the application of several different external stimuli, such as chemical wetting,[39-41] magnetic field manipulation,[42, 43] and mechanical stress.[44] The major disadvantage of many strategies based on invisible photonic crystal patterns reported in the literature is that the initial encrypted state is already colored, as attributed to their inherent micro-/nanostructural periodicity, which is why these materials always rely on a complete relaxation back to the initial state to ensure the invisibility of the encrypted information. However, slight inhomogeneity in the different areas of the patterns cannot be reproducibly eliminated and it is therefore difficult to suppress failure in the reversible encryption process.

In the present study, highly transparent photonic crystal (TPC) films with engineered solvent-responsive optical properties are generated by utilizing polymeric particles and surrounding matrix material with perfectly matched refractive indices (i.e. *isorefractive*); hence resonant scattering at the underlying photonic crystal structure is completely suppressed in the initial state. The as-prepared TPC films are highly transparent (>99% transmittance); as the films are swollen with mixtures of ethanol (EtOH) and water (H_2O), having a comparably lower refractive index, the indices of particles and matrix material change at different rates. The result is increasingly strong resonant light scattering that causes encrypted structural color patterns to progressively appear, while the film transmittance is simultaneously reduced. The switch between transparent and colored states is fully reversible over many cycles, which leads to the complete appearance and disappearance of encrypted photonic patterns without affecting the structural and optical integrity of the films. Moreover, the solvatochromic

mechanism can be adjusted over a wide range of action by tuning the initial particle size, as well as the composition of the solvent mixtures.

This polymer-based TPC approach described here has the great advantage of easily scalable large-area processing (compatible with standard press or roll-to-roll fabrication, followed by UV irradiation) and very clear revelation (change from transparent to colored state) compared with previous methods. These TPCs take the macroscopic form of a stable, mechanically robust, viscoelastic solid and should also be transferable onto tractable media such as fabrics and papers, as demonstrated recently in the homologous "polymer opals" system.[45, 46]

2. Experimental and Materials

TPC films, with typical thicknesses of 100-150 microns, were generated from the polymer core-shell batch materials, using a heated-press compression and melt-flow method; full details of materials synthesis, film production and characterisation methodology are given in this section.

Materials: Methyl methacrylate (MMA), ethyl acrylate (EA) and butanediol diacrylate (BDDA) were obtained from Shanghai Sinopharm Chemical Reagents Co. Ltd. (China), allyl methacrylate (ALMA) and benzyl methacrylate (BzMA) from Aladdin Chemical Co. Ltd. (China) and Dowfax 2A1 from Dow Chemical Company (China). All other chemicals were purchased from Shanghai Sinopharm Chemical Reagents Co. Ltd. (China) and Aladdin Chemical Co. Ltd. (China) as well, and used as received. Prior to use in the emulsion polymerization, the stabilizers hydroquinone monomethylether and brenzcatechine monomethylether were removed from the monomers. For this purpose, MMA, EA, BzMA ALMA and BDDA were destabilized using an alumina oxide (basic, 50-200 μ, Aladdin Chemical Co. Ltd.) column.

Methods: Transmission electron microscopy (TEM) was performed on a FEI CM20 at an operating voltage of 200 kV. Dynamic light scattering (DLS) measurements were conducted on a Malvern Zetasizer Nano ZS at 25 °C. Field emission scanning electron microscopy (FESEM) was performed on a Zeiss GeminiSEM 500 at an operating voltage of 3 kV. Atomic force microscopy (AFM) measurements were performed in the tapping mode using a Bruker Multimode Nano 4 atomic force microscope equipped with a silicon cantilever. UV crosslinking of the films was done by a BLTUV industrial-type mercury lamp (Dongguan

Ergu Photoelectric Technology Co. Ltd.). The output power of the lamp was 1000 W. Transmission spectra were measured by using a Shimadzu UV 3600 plus UV-Vis spectrophotometer. Reflection spectra were recorded using an Ideaoptics PG2000 pro Vis-NIR fiber spectrophotometer. For the reflection measurements Ideaoptics DH2000-BSC deuterium/halogen lamp was used. Angle-dependent reflection measurements were carried out using a custom-build goniometer setup. Reflection measurements in EtOH/H_2O mixtures as a function of EtOH concentration were carried out at normal light incidence. Swelling and de-swelling of the films was tracked by immersing the film in EtOH and subsequent drying at room temperature. Reversible switching was followed by recording reflection spectra after each cycle.

Core-shell particle synthesis: Under argon, a 1 L flask equipped with stirrer and reflux condenser was filled at 75 °C with a cold monomer emulsion consisting of 280 g deionized water, 1.20 g BDDA, 2.80 g MMA and 0.15 g sodium dodecylsulfate (SDS). The polymerization was initiated immediately by adding 50 mg sodium bisulfite, 150 mg sodium peroxodisulfate (SPS), and 50 mg sodium bisulfite in this sequence (PMMA seed). After 10 min, a monomer emulsion containing 23.1 g BDDA, 53.9 g MMA, 0.23 g SDS, 0.22 g Dowfax 2A1, 0.4 g KOH and 90 g water was added continuously over a period of 3.5 h (PMMA core). After 30 min of reaction time, 50 mg SPS were added. After additional 15 min, a monomer emulsion containing 3 g ALMA, 4 gBzMA 21 g EA, 0.05 g SDS, 0.21 g Dowfax 2A1, 0.1 g KOH and 32 g water was added continuously within 50 min. After 15 min of reaction time, a monomer emulsion of 112.6 g EA, 27.4 g BzMA, 0.40 g SDS, 0.2 g KOH and 160 g water was added continuously over a period of 4.5 h (PEA-co-PBzMA shell). After additional 60 min, the product is cooled to room temperature. The synthesis yielded particles with an average diameter of 187 nm. Other particle sizes were obtained by varying the amount of SDS in the seed stage: 0.100 g SDS yielded particles with a diameter of 225 nm, while 0.075 g of SDS yielded particles with a diameter of 248 nm.

Film Preparation: For preparation of the transparent photonic crystal (TPC) films, the particle dispersion (containing 33 wt % polymer) was coagulated in methanol, filtered and dried to isolate the polymer. The polymer was mixed with 5 wt% benzophenone in a Haake Rheomix OS lab compounder equipped with a Haake PolyLab OS Rheodrive 7 at 120 °C. A 1 g portion of the rubbery polymer was covered with PET film and heated to 140°C between the plates of a SLIMC platen vulcanization press. Melt flow was induced by applying a pressure of 100 bar for 3 min, resulting in TPC films of about 10 cm in diameter, and with thicknesses of 100-150 microns. Films could then be easily peeled from the PET backing, to generate free-standing

films, with the flexible visco-elasticity characteristic of the polymeric components.[47] For subsequent cross-linking, the films were irradiated at a distance of 15 cm from the UV-A light source for 1 min. The use of benzophenone as a UV-initiated organic cross-linker has been used previously as a standard method of crosslinking the shell (polyacrylate) components (see Ding *et al*.,[48]); the free radicle mechanisms involved will result in covalent bridging bonds to be formed locally between adjacent particles. Spatially resolved crosslinking has then been carried out by placing a metal pattern with the emblem of Fudan University on the film to protect parts of the film from irradiation with UV light.

3. Results and Discussion

3.1. Sample Characterisation

The TPC films with a refractive index contrast $\Delta n = 0$ between the particles and the surrounding matrix material are fabricated from monodisperse core-shell particles composed of a polymethyl methacrylate (PMMA) core and a copolymer shell of 80 wt% polyethyl acrylate and 20 wt% polybenzyl methacrylate (PEA-co-PBzMA), synthesized using similar emulsion-polymerisation procedures for core-shell particles reported previously.[49, 50] **Figure 1a** shows representative transmission electron microscope (TEM) images of PMMA@PEA-co-PBzMA particles with a final diameter of 225 nm (Figure S1). It should be noted that these hard-soft core-shell particles already tended towards film formation during TEM sample preparation. Similar products with 187 nm and 248 nm respectively (Figure S1, Figure S2), are also available via the same procedure. This precursor material is then compounded with 5 wt% of photo-initiator (benzophenone) and pressed at elevated temperature and pressure, whereby the PEA-co-PBzMA shell material merges into a continuous molten matrix and the PMMA cores shear assemble into a highly ordered colloidal crystalline lattice structure with the (111) plane parallel to the sample surface.[51] Whilst the core-shell particles thus do collectively form a crystalline structure of hard spheres in a softer matrix, it is important to recall that the two components are chemically grafted, so no distinct fluid phase forms during the sample synthesis via shear-ordering, and the integrity of individual particles is maintained

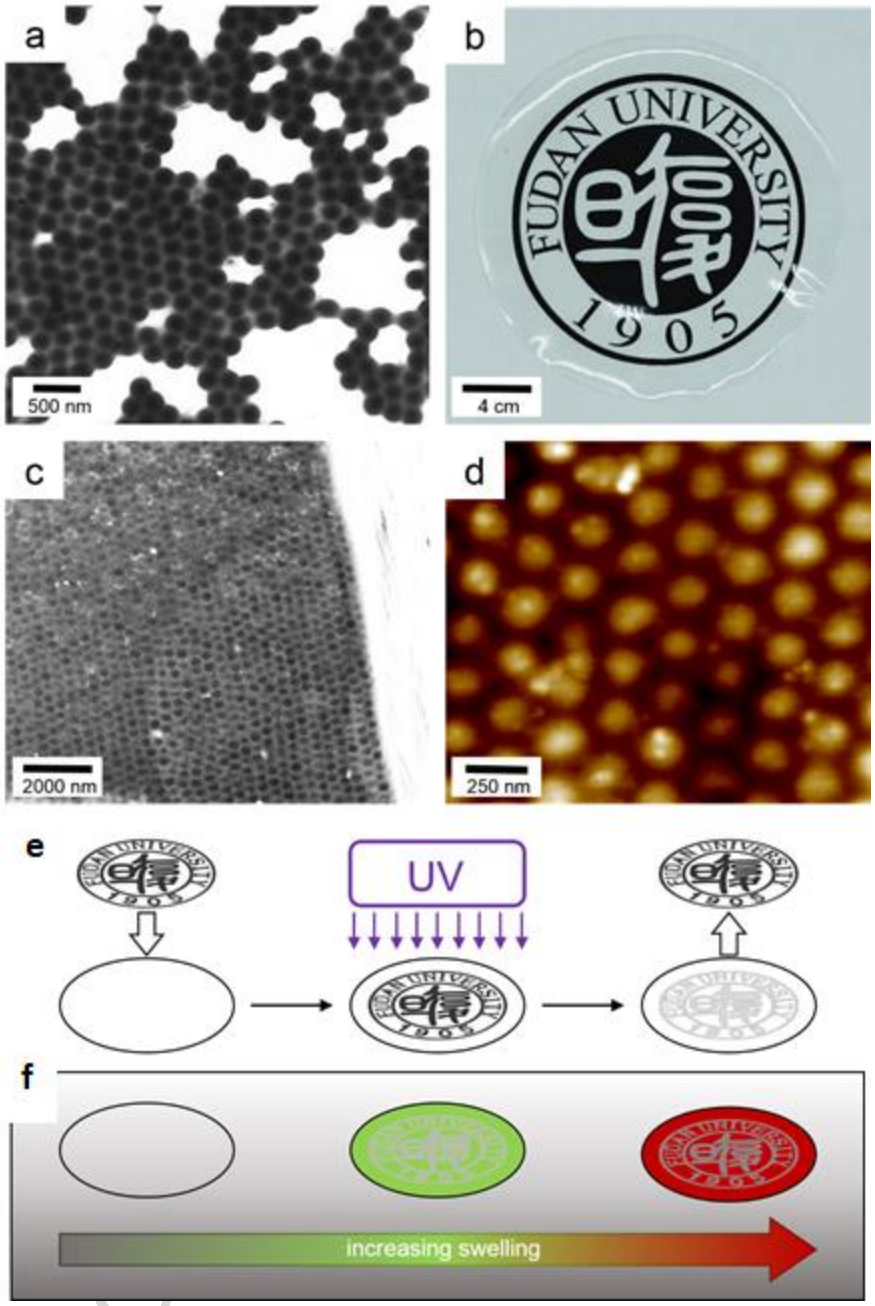

Figure 1. (a) Representative TEM image of PMMA@PEA-co-PBzMA core-shell particles with a diameter of 225 nm. (b) Image of the TPC film prepared from 225 nm particles on a black and white background of the logo of Fudan University revealing the high transparency of the film. (c) SEM image of a cross-section of the TPC film indicating the high ordering of the PMMA particles inside the P(EA-co-BzMA) matrix. (d) AFM image of the surface of the TPC film showing the hexagonally ordered (111) plane of the photonic crystal structure. (e) Schematic of the printing of invisible photonic patterns on TPCs, and (f) revealing the encrypted patterns by immersing in solvents.

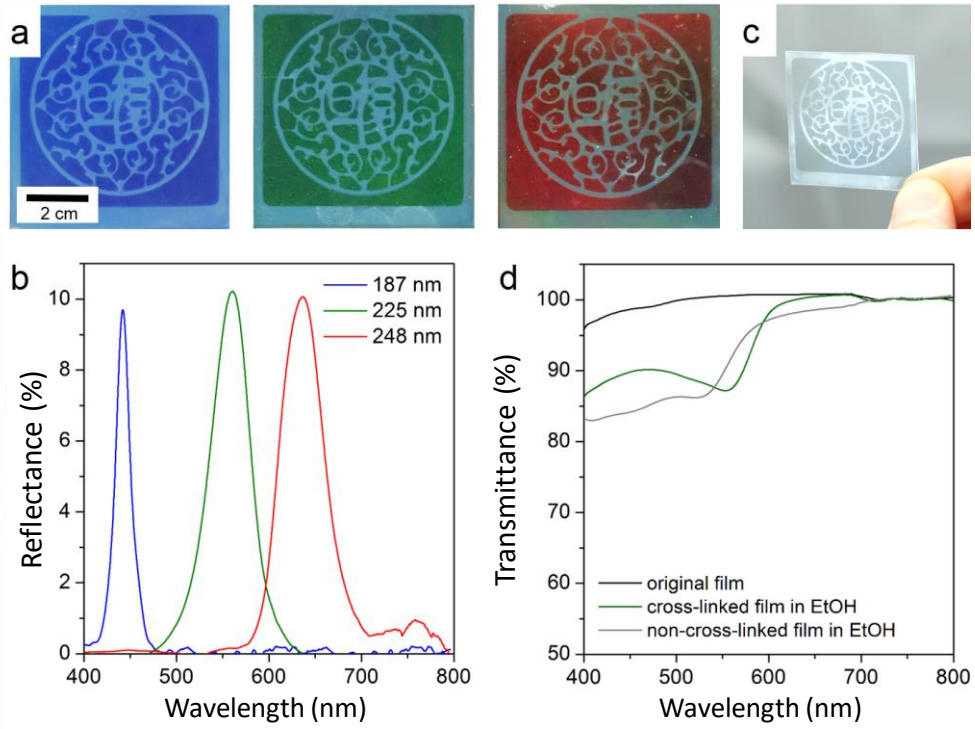

Figure 2. (a) Images of TPCs made from PMMA@PEA-co-BzMA with diameters of 187 nm (blue), 225 nm (green), and 248 nm (red) with revealed patterns after immersing in EtOH. The pre-swollen films have typical thicknesses of 100-150 microns. (b) Reflection spectra of the swollen TPCs made from PMMA@PEA-co-BzMA of different sizes. (c) Image of the green TPC showing the initial transmission color of the film. (d) Initial transmission spectra of the green TPC and the cross-linked and non-cross-linked film areas after immersing in EtOH.

Since the refractive index of PEA-*co*-PBzMA is engineered to be exactly matched to that of PMMA, the as-prepared films are highly transparent in the visible and near infrared (Vis–NIR) spectral range (400-800 nm), as seen in Figure 1b. However, it is commensurately difficult to discern the highly-ordered colloidal crystalline structure due to the lack of structural colors. To verify this, a more detailed investigation of the nanostructure is carried out using scanning electron microscope (SEM) and atomic force microscope (AFM) (see Figure 1c, d). The SEM image of a cross-section of the corresponding film sample (Figure 1c) reveal the ordered layers of PMMA particles embedded in the PEA-*co*-PBzMA material, while hexagonally arranged PMMA particles (111 plane) are clearly visible in the AFM image (Figure 1d) verifying that highly ordered TPC films are indeed accessible via these methodologies. As shown as a demonstration in Figure 1e, by spatial UV-induced crosslinking by using a photomask, invisible Chinese characters of the emblem of Fudan University can be encrypted into the TPCs. Because of the efficient cross-linking in the UV irradiated regions, they develop less swelling and more structural integrity than non-irradiated regions when immersed in solvents. Consequently, strong structural color is observed in the

irradiated compared with non-irradiated regions, leading to a high contrast accompanied with a clear revelation of the encrypted images (Figure 1f).

The basic procedure for message revelation is to immerse the TPCs in a solvent, whose refractive index is comparably higher or lower to induce distinct refractive index contrast. To demonstrate this experimentally, using suitability compatible polar solvents, we chose EtOH (n_{EtOH} = 1.36) as the solvent to have high contrast with respect to the PMMA core particles (n_{PMMA} = 1.49). Upon immersing the TPCs in EtOH, two optical phenomena are observed: i) switching from transparent to a colored state, and ii) appearance of uniform colorless patterns on the structural colored background (Video S1, Video S2). Accordingly, blue, green, and red films are obtained from TPC films made from precursor particles with diameters of 187, 225, and 248 nm, respectively, as shown in **Figure 2a**.

The reflection spectra for these three TPC films (Figure 2b) show resonant reflection peaks at 441 nm (blue), 561 nm (green), and 636 nm (red), owing to the highly-ordered colloidal crystalline structure. The same green film clearly reveals patterns in transmission, as shown in Figure 2c, as a white light illumination source is observed through the TPC film. A typical transmission spectrum for the TPC film (Figure 2d) shows ~100% transmittance for the initial film over almost the whole Vis-NIR spectral range, as well as a very high transmittance of the cross-linked film areas after swelling with EtOH, of around 99% for wavelengths longer and 88% for wavelengths shorter the Bragg peak. In contrast, the transmittance in the non-cross-linked areas is significantly reduced to 98% at longer and 84% at shorter wavelengths, as shown in Figure 2d. The TPC films exhibit significant Bragg peak reflectivity in the cross-linked areas, as well as the high transparency at wavelengths outside the Bragg peak, as clearly visible in the transmission measurements. However, the non-cross-linked areas show a broadband scattering, which suggests some loss of crystallinity during swelling.[52] We note that the loss of order in the non-cross-linked parts does not affect the invisibility and the revealing processes of the encrypted information, since the initial transparent state does not depend on the nanostructure. Despite the relatively small refractive index contrast after swelling (see later section on *Modelling and Simulation*), a high visual contrast for the revealed encrypted images can be achieved owing to the 100s of ordered layers of TPC film and the differences in structural integrity accompanied by different swelling behaviors of irradiated and non-irradiated film regions. Indeed, simultaneous changes in reflectivity and transmission are lower compared to other colloidal (high index-contrast) photonic crystals, due to the unusual structural color mechanism that only emerges after swelling with solvents.

However, the distinct appearance of the photonic patterns can be easily observed and distinguished by the naked eye, which is the basic prerequisite for the use of our material in optical sensors and security applications.

The evolution of reflection spectra is recorded to verify the visual observations, and to explain the mechanism of photonic pattern visibility, understanding of which is required for use of the TPCs within effective anti-counterfeit devices. As spectra illustrate, two different effects can be observed in the TPC films: i) a change from transparent to a colored state due to the increase of the refractive index during swelling, and ii) red-shifting of the structural color with increasing solvent swelling because the lattice constant increases, as does the plane spacing in the normal direction to the film surface. However, the spatially-resolved UV cross-linking produces different swelling properties in irradiated compared to non-irradiated film areas and, therefore, both areas show different optical response. As a result, a strong variation of the reflection spectra between cross-linked and non-cross-linked regions can be observed (Figure 1f). Both the reflection spectra for the cross-linked as well as for the non-cross-linked regions show common characteristics, which include two superimposed reflection peaks and their merging until the film swelling is completed after 5 min (**Figure 3a, b**).

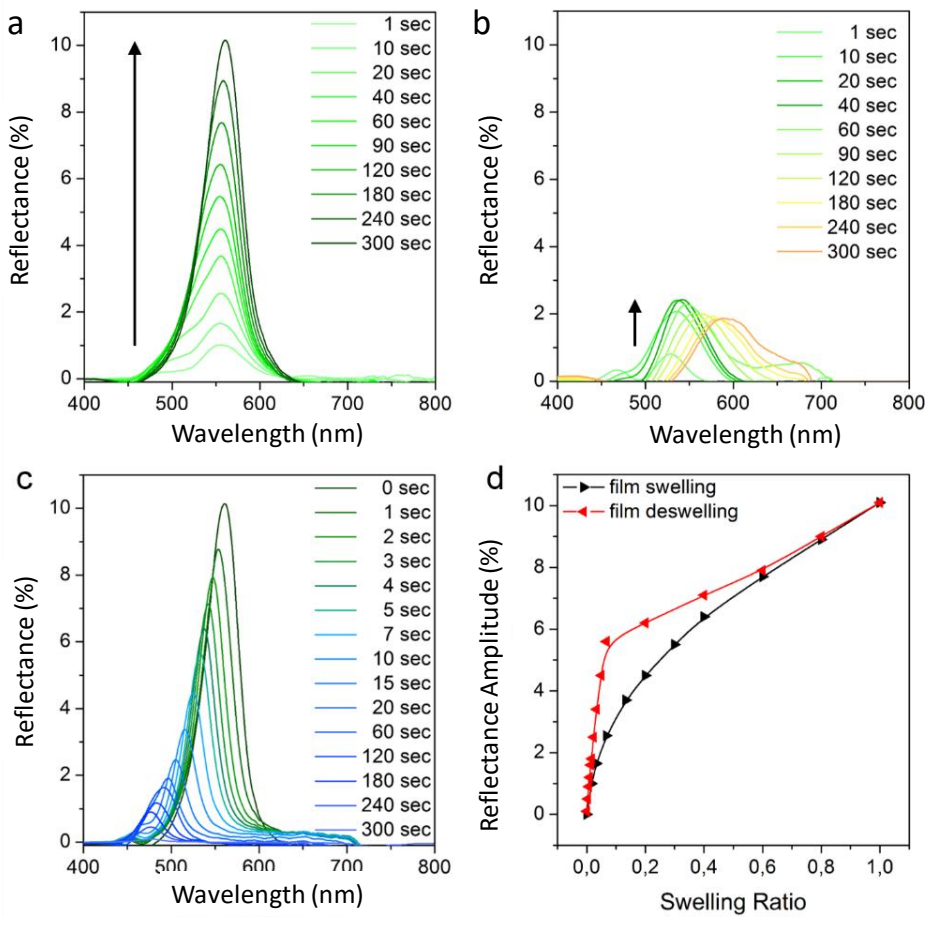

Figure 3. Evolution of reflection spectra of (a) cross-linked, and (b) non-cross-linked film areas after immersing the green TPC in EtOH. (c) Evolution of reflection spectra during evaporation-induced de-swelling of the cross-linked film areas of the green TPC. (d) Hysteresis loop of the swelling/de-swelling of the green TPC with EtOH.

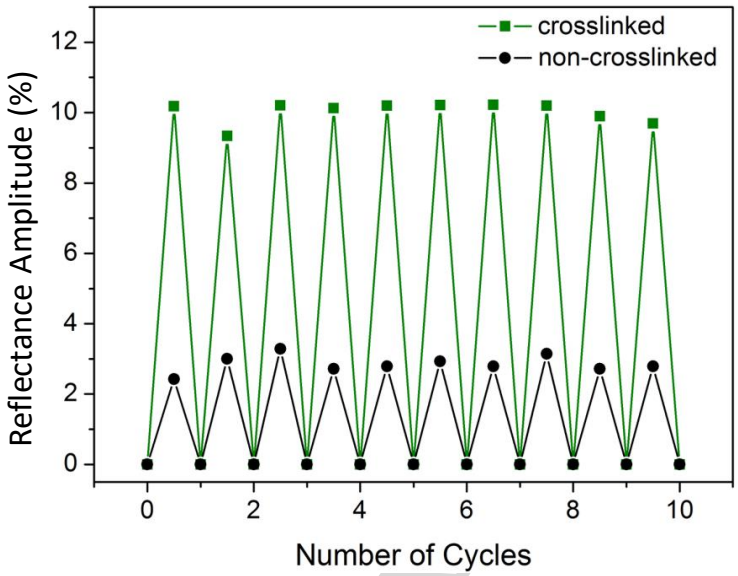

Figure 4. (a) Changes of reflection intensity of cross-linked and non-cross-linked regions under 10 cycles of swelling and de-swelling with EtOH.

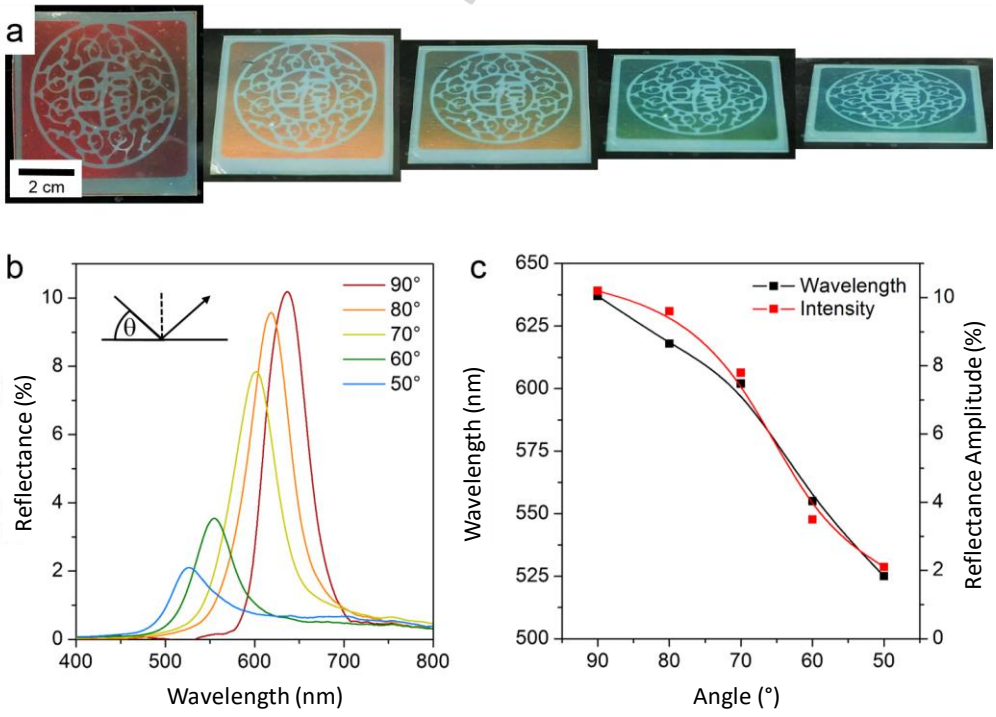

Figure 5. (a) Images of the red TPCs under different angles of view (90°, 80°, 70°, 60°, 50° from left to right). (b) Reflection spectra, and (c) changes of reflection wavelength and intensity with the angle of light incidence.

This behavior can be attributed to the appearance of non-uniform distribution of EtOH in the surface layer and inner layers until a balanced swelling state is achieved.[53] In this state, the equilibrium structure after solvent infiltration has gone to completion, which experiments show can take a finite time to be attained. However, the reflection intensity in the cross-linked parts of the film strongly increases, which originates from the increasing refractive index contrast, while the peak wavelength shifts only slightly due to the structural integrity (Figure 3a). In contrast, the reflection spectra for the non-cross-linked film areas show only slight changes of the reflection intensity, which initially rises slightly and then drops again, accompanied by a red shift and a strong broadening of the reflection peak (Figure 3b). In the non-cross-linked samples, we note that the decrease in reflection intensity as well as the broadening of the peak is due to a loss of crystalline order derived from the lattice deformation during swelling. However, the large difference in the peak evolution between irradiated and non-irradiated regions means that the invisible images are clearly observable already after several seconds and the contrast progressively increases until swelling is completed (Video S1, Video S2).

To understand further the structural changes and optical properties of the TPCs and to gain insight into potential practical applications, the evolution of reflection spectra during de-swelling is also followed. Surprisingly, during evaporation-induced de-swelling, the initial reflection peak located at 561 nm is blue-shifted to 475 nm, while the peak intensity significantly decreases and completely vanishes after 5 min of evaporation (Figure 3c). This large difference in the optical response between swelling and de-swelling can be attributed to the uniform evaporation of EtOH out of a balanced swollen state of the TPCs. Interestingly, although this apparent hysteresis is present in the reflection intensity for increasing and decreasing swelling ratio (Figure 3d), after complete evaporation of EtOH the initial transparent state of the TPC film is totally restored.

The TPC patterns can reversibly enabled and disabled many times by cyclical swelling and de-swelling with EtOH. **Figure 4** shows the progression of the reflection intensity in such a swelling/de-swelling cycle. During each cycle, the entire TPC is switched to its structural colored state by immersing into EtOH and then released to its initial transparent state by solvent evaporation. As demonstrated, the reflection intensity of the irradiated and non-irradiated regions shift reversibly up and down with good reproducibility. In spite of the partial loss of structural order in non-cross-linked regions of the film, the reversible switch between transparent and colored states is fully reversible over many cycles, which leads to the

complete appearance and disappearance of encrypted photonic patterns without affecting the optical integrity of the film.

In respect of the putative practical application as a security feature, the visibility of the patterns over a wide range of viewing angles must be ensured. Each of the TPC films shown in Figure 2a exhibited bright reflected colors, as well as a good optical contrast of the revealed patterns under normal light incidence. As a demonstration of the visibility of the patterns at different viewing angles, we used the red TPC film as example for an anti-counterfeit pattern. The film exhibits a bright back-reflection color as shown in the main image in **Figure 5a**. For lower incident and reflection angles, the color of cross-linked regions is blue-shifted (in accordance with the expected out-of-plane periodicity[25]) as the angle of incident light is decreased from 90° to 50° and the colored pattern remains fully visible over all observed angles of view. As the angle is decreased, a shift of the Bragg peak is clearly visible in reflection spectra, while the reflection intensity decreases slightly (Figure 5b). The significant blue shift of the Bragg peak with smaller incident angle corresponds to the expectations according to the Bragg equation (Figure 5c), while the reflection intensity simultaneously decreases with increased measurement obliquity as expected.

With regard to solvatochromic behavior and subsequent usability for optical sensing applications, the optical response of prepared TPC films to the changing solvent environment is investigated. In order to demonstrate this capability experimentally, samples are covered and soaked by specific solvent mixtures. Hence, different solvent response can be obtained by the osmotic pressure of the solvents according to Figure 1f. For this purpose, the TPCs are wetted by different EtOH/H_2O mixtures, resulting in a gradual revelation of the encrypted images on the TPCs (**Figure 6a**). With increasing content of EtOH, a progressively increasing contrast and clear revelation of the encrypted images, as well as a red shift of the pattern color, is clearly visible. The increasing contrast and the red-shift is due to both the increase of the refractive index contrast as well as the lattice constant caused by swelling from the solvent, with pure EtOH giving the best pattern contrast. Figure 6b shows the corresponding reflection spectra when the TPCs are immersed in different solvent mixtures. With increasing content of EtOH, the Bragg peak strongly red-shifts by more than 100 nm (Figure 6c), which means a change from 538 nm (green) to 640 nm (red) of the Bragg peak. An accompanying increase in reflection intensity (Figure 6c) and enhanced visual color brilliance can be observed, with the red-shift due to a distinct swelling as the volume fraction of low refractive index EtOH/H_2O is increased in the matrix material. This distinct appearance of the photonic

patterns demonstrates that the response of the TPC film to EtOH/H_2O can be easily observed by the naked eye (Figure 6a). The switchable optical properties obtained here are thus very promising for applications in both anti-counterfeiting devices as well as colorimetric ethanol sensors, for instance in alcoholic beverages. The large *fractional* changes in optical response (i.e. resonant reflectivity going from ~0 to 10%) also suggest that these TPC films could possibly be used as active components within integrated optoelectronic sensors involving photodiodes or light-dependent resistors.

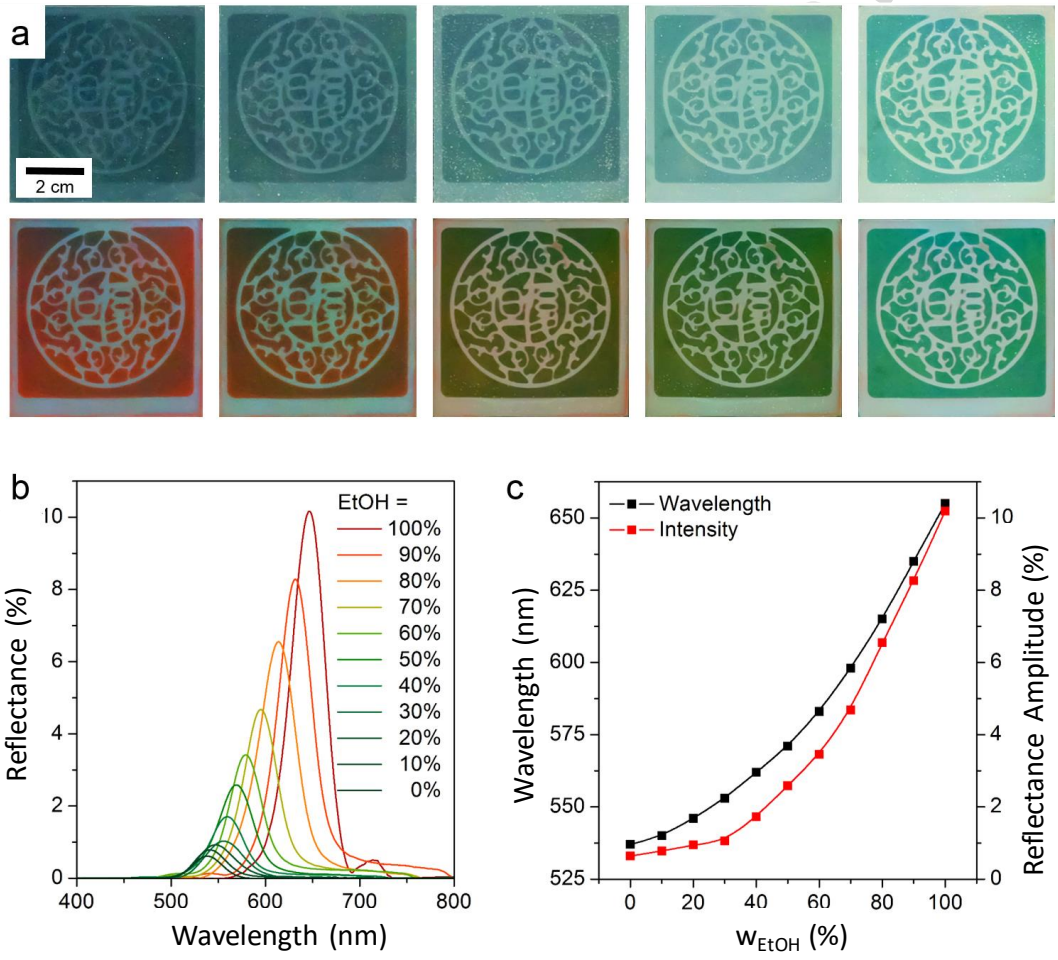

Figure 6. (a) Images of a red TPC immersed in different EtOH/H_2O mixtures (0%, 10%, 20%, 30%, 40%, 50%, 60%, 70%, 80%, 90% EtOH, *clockwise* from top left to bottom left). (b) Reflection spectra, and (c) changes of reflection wavelength and intensity with the EtOH content in the solvent mixtures.

3.2. Modelling and Simulation

To elucidate further the role of index-contrast in the development of TPC structural color, we have developed a multilayer quasi-model of the opaline structures, as per earlier studies.[54,

55] Representing the periodicity of the opals, rather than their exact 3-dimensional structure, this consists of non-absorbing λ/4 layer-pair stacks of the high and low *n* components giving resonance at central λ as determined by the experimental data. In addition, the layers have a Gaussian-distributed thickness error of width γ, which accounts for deviations from perfect crystalline order within the photonic crystal, which we know must be present to some degree in the TPCs with finite optical resonance bandwidth. The reflectivity spectra of these model structures are calculated using a transfer-matrix method averaged over many cycles,[56] using suitable parameters.

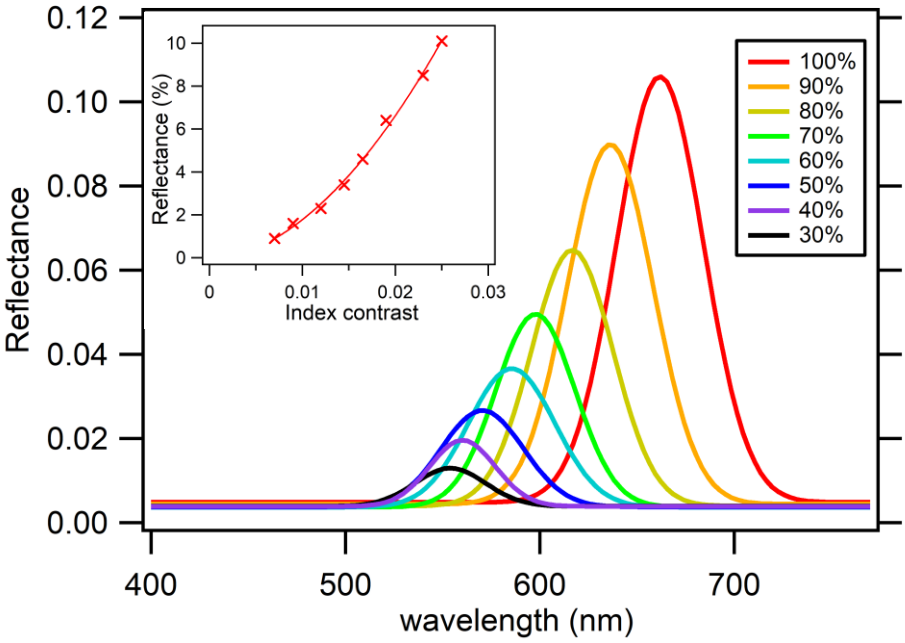

Figure 7. Simulated reflectance spectra of opal films, based on a corresponding multilayer quasi-model, with parameters 50 layer-pairs, Gaussian layer-disorder parameter γ = 15nm, and extinction coefficient α = 0. Peak wavelengths were set as per the experimentally measured values, ranging from 660 nm for the 100% EtOH/H_2O infusion, to 552 nm for the 30% case; the EtOH content in the solvent mixtures for each sample is shown in the legend. (Inset) peak reflectivity values of spectra are plotted against the derived values of refractive-index contrast (Δn), with a quadratic trendline added for clarity.

Representative simulation results are shown in **Figure 7;** as the TPC opaline films simulated here are similar in nature and preparation methods to the earlier reports of Spahn, Finlayson *et al.*,[57, 58] intuitively similar values are also used for γ (15nm, or ~ 7-8% of layer thickness variation) and overall multilayer thickness. The index-contrast values (Δn) are set such that the lower index component is n_{PMMA} - Δn, with the higher index component thus set at 1.49. Δn is then varied in order to match the simulated reflectance with the experimental value

studied and this is seen to give realistic Lorentzian spectral profiles, with FWHM values of 50–60 nm. The critical dependence of the simulated/observed peak intensities on Δn is clearly shown in Figure 7 (inset). Whilst Fresnel theory predicts a quadratic dependency of reflectivity on Δn from perfectly ordered photonic crystals, in these opaline systems coherent superposition at the reflectance peak is disrupted by the cumulative phase shifts from thickness fluctuations (disorder) since the light penetrates to depths of 10-100s of layers in such low Δn systems. Previously, a roughly linear dependence in the Δn range of 0.05 to 0.2 has thus been observed, however the present TPC samples offer a convenient way of studying this very low Δn regime ($\Delta n/n \leq 2\%$) in closer detail. The polynomial splice trendline fitted to the data shows a trend that is marginally super-linear, with elements of both a linear term and a quadratic term with small weighting, again indicating the complexity of model required for a full understanding of the interplay of disorder and index contrast in the low Δn regime. We note with interest some recent studies of the theoretical condition for transparency in mesoporous layered optical media,[59] especially in the context of stimuli-responsive switching.

4. Conclusion

In conclusion, we have presented a convenient fabrication of large-area transparent photonic crystal (TPC) films out of polymer core-shell particles, with perfectly balanced refractive indices, that can be completely and reversibly switched between a transparent state and a structurally colored state. Outline simulations confirm the mechanisms of solvatochromism as the core-shell refractive index contrast increases, and illustrate the rich underlying optics involving an interplay between Δn, solvent swelling, and inherent disorder in the crystalline structures. Moreover, these TPCs can be spatially cross-linked by UV irradiation, giving invisible photonic patterns with different solvent response compared to non-cross-linked regions. Corresponding encrypted images appeared as versatile colorful patterns onto the photonic crystal structure by simply immersing in solvents.

We finally note how the transferable modular nature of these synthesis methods offers many possible variations in design, in terms of solvent activity/permeability, refractive index, and, potentially, multi-functionality of the polymer components. There are also recently reported developments in the technology of visco-elastic shear-assembly of such composite particles;

in particular, the so-called bending-induced oscillatory shear (BIOS) process,[60, 61] which promises yet further future improvements upon the crystalline ordering of engineered TPC films and the achievable optical response.

This facile approach enables the generation of TPC films with stored secret information accompanied by fascinating and fully reversible tunable optical properties. These materials and thin-film generation methods offer a great many advantages over more “monolithic” designs for switchable structural colour in opals and photonic crystals; they are easily scalable and transferable in preparation, and are highly stable/cyclic-able and physically robust. We thus consider these polymer opaline TPCs as promising photonic material for sensor applications, the storage of secret information, and for anti-counterfeit devices on (e.g.) bank notes, passports, credit cards, merchandise and brand labels.

Acknowledgements
The authors acknowledge financial support from the National Science Foundation of China (Grant No. 51721002, 51633001, 21474017, 21507011, 21677037), the Ministry of Science and Technology of the People's Republic of China (Grant No. 2016YFE0112200), the State Key Project of Research and Development (Grant No. 2016YFC1100300), the Natural Science Foundation of Shanghai (Grant No. 17ZR1440200), and the China Postdoctoral Science Foundation funded project No. KLH1829019. CEF acknowledges the ongoing support of the Welsh European Funding Office (WEFO) programmes KESS-2 and SPARC-II. We thank Dr. Qibin Zhao for helpful discussions and technical support with SEM measurements.

Data Availability
The raw data required to reproduce these findings are available to download from doi:10.17632/4wpdfb5cb2.1. The processed data required to reproduce these findings are available to download from doi:10.17632/4wpdfb5cb2.1.

References

[1] B. Hardwick, W. Jackson, G. Wilson, A.W.H. Mau, Advanced Materials for Banknote Applications, Advanced Materials 13(12-13) (2001) 980-984.
[2] E.L. Prime, D.H. Solomon, Australia’s Plastic Banknotes: Fighting Counterfeit Currency, Angewandte Chemie International Edition 49(22) (2010) 3726-3736.
[3] B. Yoon, J. Lee, I.S. Park, S. Jeon, J. Lee, J.-M. Kim, Recent functional material based approaches to prevent and detect counterfeiting, Journal of Materials Chemistry C 1(13) (2013) 2388-2403.
[4] G. von Freymann, V. Kitaev, B.V. Lotsch, G.A. Ozin, Bottom-up assembly of photonic crystals, Chem Soc Rev 42(7) (2013) 2528-54.

[5] F. Li, D.P. Josephson, A. Stein, Colloidal assembly: the road from particles to colloidal molecules and crystals, Angewandte Chemie International Edition 50(2) (2011) 360-388.
[6] N. Vogel, M. Retsch, C.A. Fustin, A. Del Campo, U. Jonas, Advances in Colloidal Assembly: The Design of Structure and Hierarchy in Two and Three Dimensions, Chem Rev (2015).
[7] J.F. Galisteo-López, M. Ibisate, R. Sapienza, L.S. Froufe-Pérez, Á. Blanco, C. López, Self-Assembled Photonic Structures, Advanced Materials 23(1) (2011) 30-69.
[8] L. Gonzalez-Urbina, K. Baert, B. Kolaric, J. Perez-Moreno, K. Clays, Linear and nonlinear optical properties of colloidal photonic crystals, Chem Rev 112(4) (2012) 2268-85.
[9] S. Asher, J. Weissman, A. Tikhonov, R. Coalson, R. Kesavamoorthy, Diffraction in crystalline colloidal-array photonic crystals, Physical Review E 69(6) (2004) 066619.
[10] Y. Vlasov, M. Deutsch, D. Norris, Single-domain spectroscopy of self-assembled photonic crystals, Applied Physics Letters 76(12) (2000) 1627-1629.
[11] M. Serpe, Y. Kang, Q. Zhang, Photonic Materials for Sensing, Biosensing and Display Devices, Springer, Switzerland AG 2016.
[12] R.A. Potyrailo, R.K. Bonam, J.G. Hartley, T.A. Starkey, P. Vukusic, M. Vasudev, T. Bunning, R.R. Naik, Z.X. Tang, M.A. Palacios, M. Larsen, L.A. Le Tarte, J.C. Grande, S. Zhong, T. Deng, Towards outperforming conventional sensor arrays with fabricated individual photonic vapour sensors inspired by Morpho butterflies, Nature Communications 6 (2015) 12.
[13] S. Vignolini, T. Gregory, M. Kolle, A. Lethbridge, E. Moyroud, U. Steiner, B. Glover, P. Vukusic, P. Rudall, Structural colour from helicoidal cell-wall architecture in fruits of Margaritaria nobilis, Journal of the Royal Society Interface 13(124) (2016).
[14] Z.Y. Cai, A. Sasmal, X.Y. Liu, S.A. Asher, Responsive Photonic Crystal Carbohydrate Hydrogel Sensor Materials for Selective and Sensitive Lectin Protein Detection, Acs Sensors 2(10) (2017) 1474-1481.
[15] Z.Y. Cai, N.L. Smith, J.T. Zhang, S.A. Asher, Two-Dimensional Photonic Crystal Chemical and Biomolecular Sensors, Analytical Chemistry 87(10) (2015) 5013-5025.
[16] J. Ge, Y. Yin, Responsive photonic crystals, Angewandte Chemie International Edition 50(7) (2011) 1492-522.
[17] C.I. Aguirre, E. Reguera, A. Stein, Tunable Colors in Opals and Inverse Opal Photonic Crystals, Advanced Functional Materials 20(16) (2010) 2565-2578.
[18] Y. Takeoka, Stimuli-responsive opals: colloidal crystals and colloidal amorphous arrays for use in functional structurally colored materials, Journal of Materials Chemistry C 1(38) (2013) 6059-6074.
[19] C. Fenzl, T. Hirsch, O.S. Wolfbeis, Photonic crystals for chemical sensing and biosensing, Angewandte Chemie International Edition 53(13) (2014) 3318-35.
[20] M. Qin, Y. Huang, Y. Li, M. Su, B. Chen, H. Sun, P. Yong, C. Ye, F. Li, Y. Song, A Rainbow Structural-Color Chip for Multisaccharide Recognition, Angewandte Chemie-International Edition 55(24) (2016) 6911-6914.
[21] X.-Q. Wang, C.-F. Wang, Z.-F. Zhou, S. Chen, Robust Mechanochromic Elastic One-Dimensional Photonic Hydrogels for Touch Sensing and Flexible Displays, Advanced Optical Materials 2(7) (2014) 652-662.
[22] D. Yang, S. Ye, J. Ge, From Metastable Colloidal Crystalline Arrays to Fast Responsive Mechanochromic Photonic Gels: An Organic Gel for Deformation-Based Display Panels, Advanced Functional Materials 24(21) (2014) 3197-3205.
[23] H. Kim, J. Ge, J. Kim, S.-e. Choi, H. Lee, H. Lee, W. Park, Y. Yin, S. Kwon, Structural colour printing using a magnetically tunable and lithographically fixable photonic crystal, Nat Photon 3(9) (2009) 534-540.

[24] L. Wang, J. Wang, Y. Huang, M. Liu, M. Kuang, Y. Li, L. Jiang, Y. Song, Inkjet printed colloidal photonic crystal microdot with fast response induced by hydrophobic transition of poly(N-isopropyl acrylamide), Journal of Materials Chemistry 22(40) (2012) 21405-21411.
[25] B. Michaelis, D.R.E. Snoswell, N.A.W. Bell, P. Spahn, G.P. Hellmann, C.E. Finlayson, J.J. Baumberg, Generating Lithographically-Defined Tunable Printed Structural Color, Advanced Engineering Materials 15(10) (2013) 948-953.
[26] J. Ge, J. Goebl, L. He, Z. Lu, Y. Yin, Rewritable Photonic Paper with Hygroscopic Salt Solution as Ink, Advanced Materials 21(42) (2009) 4259-4264.
[27] H. Fudouzi, Y. Xia, Photonic papers and inks: color writing with colorless materials, Advanced Materials 15(11) (2003) 892-896.
[28] H. Hu, Q.-W. Chen, H. Wang, R. Li, W. Zhong, Reusable photonic wordpad with water as ink prepared by radical polymerization, Journal of Materials Chemistry 21(34) (2011) 13062-13067.
[29] H. Lee, T. Shim, H. Hwang, S. Yang, S. Kim, Colloidal Photonic Crystals toward Structural Color Palettes for Security Materials, Chemistry of Materials 25(13) (2013) 2684-2690.
[30] L. Bai, Z. Xie, W. Wang, C. Yuan, Y. Zhao, Z. Mu, Q. Zhong, Z. Gu, Bio-Inspired Vapor-Responsive Colloidal Photonic Crystal Patterns by Inkjet Printing, Acs Nano 8(11) (2014) 11094-11100.
[31] J. Wang, L. Wang, Y. Song, L. Jiang, Patterned photonic crystals fabricated by inkjet printing, Journal of Materials Chemistry C 1(38) (2013) 6048-6058.
[32] J. Hou, H. Zhang, B. Su, M. Li, Q. Yang, L. Jiang, Y. Song, Four-Dimensional Screening Anti-Counterfeiting Pattern by Inkjet Printed Photonic Crystals, Chemistry-an Asian Journal 11(19) (2016) 2680-2685.
[33] X. Du, T. Li, L. Li, Z. Zhang, T. Wu, Water as a colorful ink: transparent, rewritable photonic coatings based on colloidal crystals embedded in chitosan hydrogel, Journal of Materials Chemistry C 3(15) (2015) 3542-3546.
[34] H.J. Seo, S.S. Lee, J. Noh, J.W. Ka, J.C. Won, C. Park, S.H. Kim, Y.H. Kim, Robust photonic microparticles comprising cholesteric liquid crystals for anti-forgery materials, Journal of Materials Chemistry C 5(30) (2017) 7567-7573.
[35] S.S. Lee, H.J. Seo, Y.H. Kim, S.H. Kim, Structural Color Palettes of Core-Shell Photonic Ink Capsules Containing Cholesteric Liquid Crystals, Advanced Materials 29(23) (2017) 8.
[36] S. Johnson , J. Joannopoulos Photonic Crystals; The Road from Theory to Practice, Kluwer Academic, Dordrecht, Netherlands, 2002.
[37] Y. Li, X. Zhou, Q. Yang, Y. Li, W. Li, H. Li, S. Chen, M. Li, Y. Song, Patterned photonic crystals for hiding information, Journal of Materials Chemistry C 5(19) (2017) 4621-4628.
[38] J. Hou, M. Li, Y. Song, Patterned Colloidal Photonic Crystals, Angewandte Chemie-International Edition 57(10) (2018) 2544-2553.
[39] I.B. Burgess, L. Mishchenko, B.D. Hatton, M. Kolle, M. Loncar, J. Aizenberg, Encoding complex wettability patterns in chemically functionalized 3D photonic crystals, J Am Chem Soc 133(32) (2011) 12430-2.
[40] R. Xuan, J. Ge, Invisible photonic prints shown by water, Journal of Materials Chemistry 22(2) (2012) 367-372.
[41] T. Ding, Q. Zhao, S. Smoukov, J. Baumberg, Selectively Patterning Polymer Opal Films via Microimprint Lithography, Advanced Optical Materials 2(11) (2014) 1098-1104.
[42] H. Hu, J. Tang, H. Zhong, Z. Xi, C. Chen, Q. Chen, Invisible photonic printing: computer designing graphics, UV printing and shown by a magnetic field, Scientific Reports 3 (2013) 1-5.
[43] H. Hu, H. Zhong, C. Chen, Q. Chen, Magnetically responsive photonic watermarks on banknotes, Journal of Materials Chemistry C 2(19) (2014) 3695.

[44] S. Ye, Q. Fu, J. Ge, Invisible Photonic Prints Shown by Deformation, Advanced Functional Materials 24(41) (2014) 6430-6438.
[45] C.E. Finlayson, J.J. Baumberg, Polymer opals as novel photonic materials, Polymer International 62(10) (2013) 1403-1407.
[46] D.R.E. Snoswell, J.J. Baumberg, Stretching the Imagination, Textiles 4 (2009) 8-10.
[47] H.S. Wong, M. Mackley, S. Butler, J. Baumberg, D. Snoswell, C.E. Finlayson, Q.B. Zhao, The rheology and processing of "edge sheared" colloidal polymer opals, Journal of Rheology 58(2) (2014) 397-409.
[48] T. Ding, G. Cao, C.G. Schäfer, Q. Zhao, M. Gallei, S.K. Smoukov, J.J. Baumberg, Revealing Invisible Photonic Inscriptions: Images from Strain, ACS Applied Materials & Interfaces 5 (2015) 10623-10632.
[49] C.G. Schafer, M. Gallei, J.T. Zahn, J. Engelhardt, G.P. Hellmann, M. Rehahn, Reversible Light-, Thermo-, and Mechano-Responsive Elastomeric Polymer Opal Films, Chemistry of Materials 25(11) (2013) 2309-2318.
[50] C.G. Schäfer, C. Lederle, K. Zentel, B. Stuhn, M. Gallei, Utilizing stretch-tunable thermochromic elastomeric opal films as novel reversible switchable photonic materials, Macromol Rapid Commun 35(21) (2014) 1852-60.
[51] O. Pursiainen, J. Baumberg, H. Winkler, B. Viel, P. Spahn, T. Ruhl, Shear-induced organization in flexible polymer opals, Advanced Materials 20(8) (2008) 1484-+.
[52] P. Ossi, Disordered Materials, Springer-Verlag, Heidelberg, Germany 2006
[53] Y. Zhang, Q. Fu, J. Ge, Photonic sensing of organic solvents through geometric study of dynamic reflection spectrum, Nat Commun 6 (2015) 1-7.
[54] C.E. Finlayson, C. Goddard, E. Papachristodoulou, D.R.E. Snoswell, A. Kontogeorgos, P. Spahn, G.P. Hellmann, O. Hess, J.J. Baumberg, Ordering in stretch-tunable polymeric opal fibers, Optics Express 19(4) (2011) 3144-3154.
[55] D. Snoswell, A. Kontogeorgos, J. Baumberg, T. Lord, M. Mackley, P. Spahn, G. Hellmann, Shear ordering in polymer photonic crystals, Physical Review E 81(2) (2010) 020401.
[56] M. Born, E. Wolf, Principles of Optics: Electromagnetic Theory of Propagation, Interference and Diffraction of Light, Pergamon, Oxford, UK, 1964.
[57] C.E. Finlayson, A.I. Haines, D.R.E. Snoswell, A. Kontogeorgos, S. Vignolini, J.J. Baumberg, P. Spahn, G.P. Hellmann, Interplay of index contrast with periodicity in polymer photonic crystals, Applied Physics Letters 99(26) (2011) 261913.
[58] P. Spahn, C.E. Finlayson, W.M. Etah, D.R.E. Snoswell, J.J. Baumberg, G.P. Hellmann, Modification of the refractive-index contrast in polymer opal films, Journal of Materials Chemistry 21(24) (2011) 8893-8897.
[59] O. Deparis, M.N. Ghazzal, P. Simonis, S. Mouchet, H. Kebaili, J. de Coninck, E.M. Gaigneaux, J.P. Vigneron, Theoretical condition for transparency in mesoporous layered optical media: Application to switching of hygrochromic coatings, Applied Physics Letters 104(2) (2014) 4.
[60] C. Finlayson, J. Baumberg, Generating Bulk-Scale Ordered Optical Materials Using Shear-Assembly in Viscoelastic Media, Materials 10(7) (2017) 688.
[61] Q. Zhao, C. Finlayson, D. Snoswell, A. Haines, C. Schafer, P. Spahn, G. Hellmann, A. Petukhov, L. Herrmann, P. Burdet, P. Midgley, S. Butler, M. Mackley, Q. Guo, J. Baumberg, Large-scale ordering of nanoparticles using viscoelastic shear processing, Nature Communications 7 (2016) 11661.

Xu Dong, Pan Wu, Christian Schaefer, Liwu Zhang and Changchun Wang contributed experimental work and results. Chris Finlayson contributed optical simulation data and co-composed the manuscript with Christian Schaefer.